Bright ionizing escape at high resolution from multiply imaged, gravitationally lensed galaxy

T. Emil Rivera-Thorsen*[1], Håkon Dahle[1], John Chisholm[2,3], Michael K. Florian[4], Max Gronke†[5], Michael D. Gladders[6,7], Jane R. Rigby[4], Guillaume Mahler[8], Keren Sharon[8], and Matthew Bayliss[9]

[1]Institute of Theoretical Astrophysics, University of Oslo, Postboks 1029, 0315 Oslo, Norway
[2]Observatoire de Genève, Université de Genève, 51 Ch. des Maillettes, 1290 Versoix, Switzerland
[3]Department of Astronomy and Astrophysics, University of California, Santa Cruz, CA 95064
[4]Observational Cosmology Lab, NASA Goddard Space Flight Center, 8800 Greenbelt Rd., Greenbelt, MD 20771, USA
[5]Department of Physics, University of California, Santa Barbara, CA 93106, USA
[6]Department of Astronomy and Astrophysics, University of Chicago, Chicago, IL 60637, USA
[7]Kavli Institute for Cosmological Physics, University of Chicago, Chicago, IL 60637, USA
[8]Department of Astronomy, University of Michigan, 1085 South University Avenue, Ann Arbor, MI 48109, USA
[9]MIT-Kavli Center for Astrophysics and Space Research, 77 Massachusetts Avenue, Cambridge, MA, 02139, USA

Young stars in the first galaxies produced far-ultraviolet ionizing photons that must have avoided absorption by the ubiquitous neutral hydrogen, escaped their host galaxies and ionized the gas between galaxies in the "Epoch of Reionization". After the Universe became transparent to these wavelengths, we would expect to find plenty of galaxies shining in ionizing light. Yet, only a small number of galaxies have so far been found to leak ionizing photons, either in the local universe[1,2,3] or at intermediate redshift[4,5,6,7]. How this light escapes the absorbing gas in galaxies, and why detections are so few and faint, remains unanswered. One key question is the extent to which ionizing photons escape through empty channels in a dense neutral gas versus escape through a tenuous haze[8,9,10,11,12]. Here, we present with unprecedented brightness, and in multiple gravitationally lensed images, the first unambiguous observation of ionizing photons escaping through a channel in a gas rich, neutral medium. Previous detections have been inconclusive regarding their mode of escape, but generally tend to suggest a scenario, in which the light escapes through a tenuous, highly ionized medium with a low content of neutral gas clumps. However, in recent years, indirect evidence has been mounting that channels through a neutral gas may account for a significant fraction of the escaping radiation[9,10,12]. Rather than being a binary either/or question, the two scenarios likely represent extremes on a sliding scale of possible gas configurations in a galaxy. With its brightness, this galaxy can help study ionizing continuum in detail, and the unusual mode of escape can set an important benchmark for future models.

On April 8th and 14th 2018 UT, the *Hubble Space Telescope* observed the extremely bright, strongly gravitationally lensed starburst galaxy PSZ1-ARC G311.6602–18.4624[13], or the Sunburst Arc[11], at redshift $z = 2.37$. The observations contain at least 12 images of ionizing Lyman continuum (LyC) leakage from one compact and extremely bright, strongly star-forming region, with signal-to-noise ratios as high as 42. We find an upper limit to the physical diameter of the LyC emitting region of ~ 160 pc, consistent with hot, star-forming regions in local galaxies[14]. We estimate a line-of-sight ionizing escape fraction of $76^{+17}_{-8}\%$, with 41% as a robust lower limit assuming a completely trans-

*eriveth@astro.uio.no
†Hubble Fellow

parent Intergalactic Medium (IGM) and at two sigma below the computed value. Variations in intergalactic transmission between neighboring images of the leaking region probe variations in the column density of neutral Hydrogen along the lines of sight of a factor of ~ 2 between sight lines separated by transverse distances as low as ~ 800 parsec (comoving) or ~ 250 pc (physical), an order of magnitude smaller than what has previously been probed, e.g. with close quasar pairs[15].

The Sunburst Arc is a single galaxy, gravitationally lensed into multiple images by a massive foreground galaxy cluster at $z = 0.44$. It is the brightest lensed galaxy known, and likely to be the brightest ever to be discovered[13]. It is young, strongly star forming, and shows no sign of an active nucleus (see fig. 4). We identified it as a strong candidate for ionizing escape based on ground-based spectroscopy obtained using the MagE spectrograph on the Magellan I (Baade) telescope[11]. These spectra show a triple-peaked Lyman α line profile with bright, narrow emission at line center, which is theoretically predicted to emerge from a perforated neutral medium[9], but had not previously been observed.

We observed the ionizing continuum using the *Wide Field Camera 3* (WFC3) on board the *HST* (proposal ID 15418, PI: H. Dahle) using the broad-band filter F275W in the UVIS2 channel. This filter aligns extremely well with the ionization wavelength of Hydrogen at the redshift of the lensed galaxy, with only 0.5% of the total throughput at wavelengths longer than the ionization limit of neutral Hydrogen; all results have been corrected for this non-ionizing contamination. We combined the F275W observations with previous observations using the *HST* Advanced Camera for Surveys (ACS) and the broad-band F814W filter (proposal ID 15101, PI: H. Dahle). At the redshift of the lensed galaxy, F814W is sensitive to non-ionizing near-UV light which emanates mainly from the same young, hot stars as the ionizing LyC but, crucially, is not absorbed by neutral Hydrogen.

In Fig. 1, we show close-up images of regions with detected Lyman continuum emission, along with an overview image of the entire lens and arc system with the cut-out regions marked. Each region is shown in both the F275W and F814W filters, with the images of the LyC emitting region marked in both filters for comparison. Note that image 5 is contaminated by the non-ionizing UV continuum from a foreground galaxy which contributes $\lesssim 10\%$ to its measured flux.

We performed photometry in both filters using the source detection and photometry software Source Extractor[16]. The measured F814W and F275W magnitudes are tabulated in table 1 along with the computed apparent escape fraction (see below) for each image.

We computed ionizing escape fractions based on theoretical models of stellar populations (see Methods section) which were fitted to non-ionizing spectra[11] of the emitting region. From these model spectra, we predicted the intrinsic flux ratios in the F275W and F814W filters, and compared these to the observed ratios (see Methods section for details). We have derived both the *relative* and *absolute* escape fractions, defined as the fraction of dust-attenuated (relative) and total (absolute) ionizing radiation that escapes the neutral gas in the galaxy. For both fractions, we caution that these are measurements along the line of sight; the configuration of this system with a perforated medium practically guarantees that these fractions are *not* related to the global escape fraction from the galaxy in a simple way.

The observed flux in F275W is the radiation surviving absorption both within the source galaxy and in the IGM. Consequently, the escape fraction we derive is the combined effect of the internal and intergalactic neutral Hydrogen (H I) $f_{\rm esc} \times T_{\rm IGM}$, which we call the *apparent escape fraction*, denoted $f^*_{\rm esc,rel}$. The maximum measured apparent escape fraction (found in knot 12 in the counterarc) forms a lower limit to the true escape fraction in the (unrealistic) case of completely transparent IGM. Conversely, the measured apparent escape fraction in image 12 provides a lower limit to the IGM transmission of $T_{\rm IGM} \gtrsim 48\%$, as lower transmission coefficients would imply an escape fraction higher than 100%.

To further constrain the escape fraction, we used the $T_{\rm IGM}$ distribution along simulated lines of sight from the literature[17], and excluded the values which would lead to an escape fraction larger than 100%. From the trimmed $T_{\rm IGM}$ distribution, we have extracted the 16th, 50th, and 84th percentile and, assuming these, computed the corresponding escape fractions for image 12 (see more detail in Methods section).

In Fig. 2, we have for each lensed image shown $f^*_{\rm esc,rel}$ as filled and $f^*_{\rm esc,abs}$ as open circles, with error bars showing the flux uncertainties (see Methods section for details) propagated in the standard way. The box-and-whiskers markers show absolute and relative escape fractions computed for image 12 based on the IGM transmission distribution, with dots showing median values, boxes making the 16th to 84th percentiles,

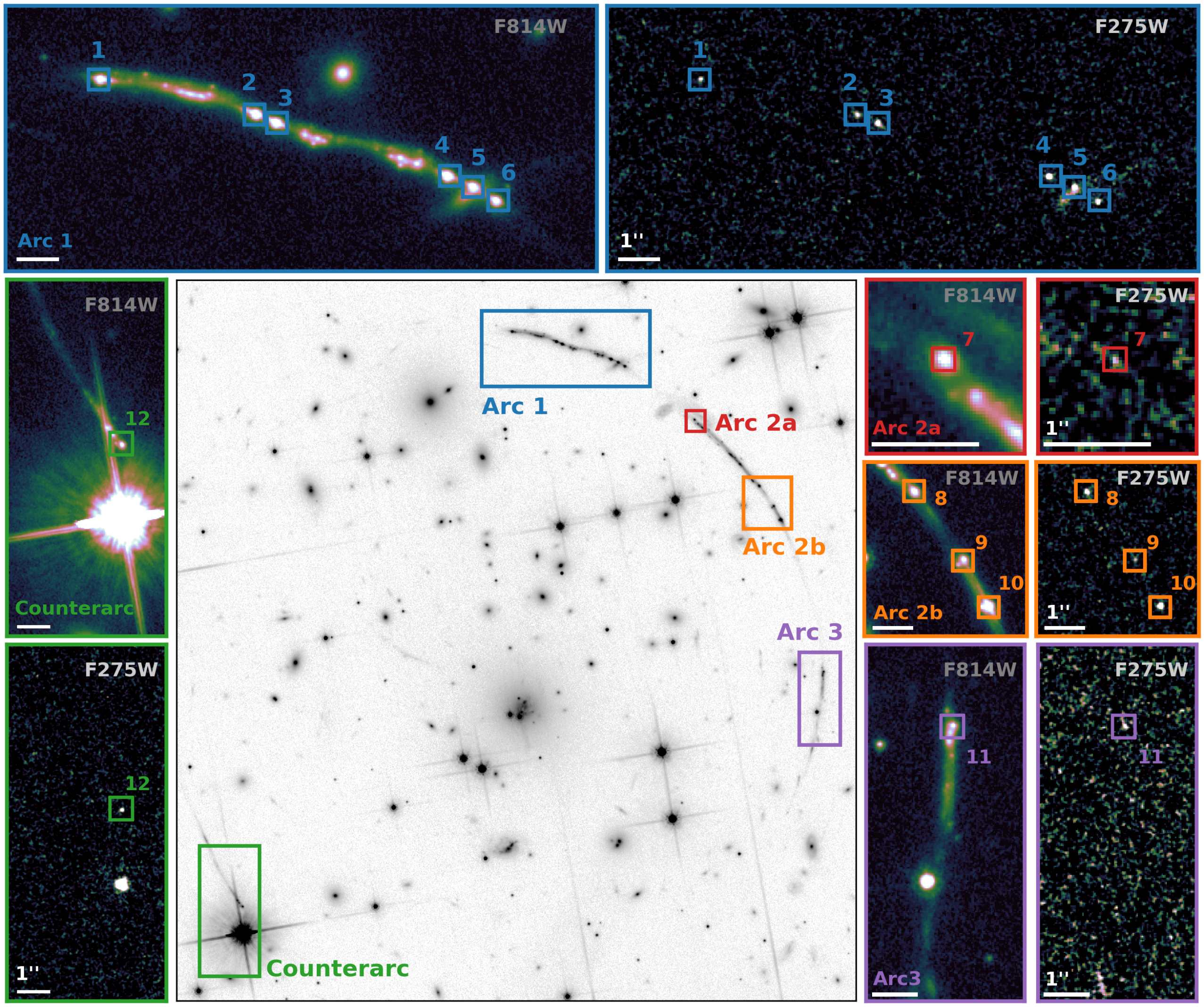

Figure 1: Pseudocolor representation of the *Hubble* exposures, zoomed in on the regions with confirmed detection of ionizing UV radiation. The F814W filter shows non-ionizing stellar UV continuum, which traces young, hot stars. Image 5 is contaminated by a foreground galaxy, which inflates its measured f^{*}_{esc} somewhat. The cutout locations are shown in the large middle panel. All panels are oriented N up, E left; scale bars mark $1''$.

and the whiskers showing the extreme wings of the distribution, bracketed by an escape fraction of 100%, and the far upper end of the T_{IGM} distribution. The filled box shows the relative, and the outlined box the absolute escape fractions. Colors correspond to the region coding in fig. 1.

Lensing models of Arc 1 (see fig. 5) show that all ionizing sources here are lensed images of the same system. Arc 3 and the Counterarc are both likely to be single, distorted images of the galaxy. Arc 2 has not yet been possible to model, but from the other arcs, we find it likely that the ionizing sources also here are images of the same system, which is supported by follow-up Magellan/MagE and MIKE spectroscopy (Bayliss et al. in prep.) of some of the images. The models place the magnification factor in Arc 1 between 10 and 30 for each image. The Lyman-continuum source is unresolved in all images, which places an upper limit on the source size at the instrument PSF of $0.09''$, corresponding to around 500 pc at the redshift of the lens. Conservatively

Table 1: Key properties of regions with detected Lyman-continuum

Image №	1	2	3	4	5	6
$m_{\mathrm{AB,\,F275W}}$ ^{a}	22.42 ± 0.09	22.29 ± 0.08	21.63 ± 0.05	21.20 ± 0.03	21.69 ± 0.05	21.88 ± 0.06
$\mathrm{S/N}_{\mathrm{F275W}}{}^{a}$	12	13	23	37	23	19
$m_{\mathrm{AB,\,F814W}}$ ^{a,b}	18.90	18.56	18.68	18.45	19.08	18.99
$f_{\mathrm{esc,rel}} \times T_{\mathrm{IGM}}$ ^{c}	18% ± 2%	15% ± 1%	31% ± 1%	37% ± 1%	43% ± 2%	32% ± 2%

Image №	7	8	9	10	11	12
$m_{\mathrm{AB,\,F275W}}$ ^{a}	23.7 ± 0.3	21.80 ± 0.06	22.80 ± 0.15	20.86 ± 0.03	23.03 ± 0.18	22.1 ± 0.08
$\mathrm{S/N}_{\mathrm{F275W}}{}^{a}$	3.7	19	7.2	42	6.2	15
$m_{\mathrm{AB,\,F814W}}$ ^{a,b}	19.67	19.17	19.43	18.34	19.85	19.65
$f_{\mathrm{esc,rel}} \times T_{\mathrm{IGM}}{}^{c}$	10% ± 3%	42% ± 2%	21% ± 3%	46% ± 1%	25% ± 4%	49% ± 3%

^{a} Observed.

^{b} All errors $\lesssim 1$ ‰.

^{c} Corrected for Milky Way dust absorption.

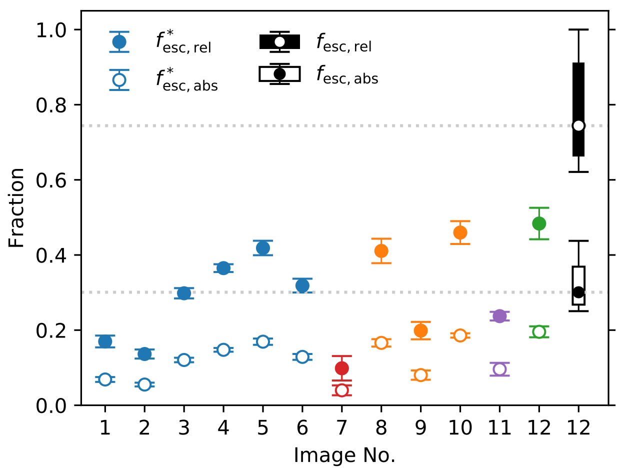

Figure 2: For each image, the fraction of the dust-attenuated and total Lyman-continuum photons that reach the telescope. Box-and-whiskers for knot 12 show the best value (dot), 16th to 84th percentile (box) and full allowed range (whiskers) of the true relative (filled) and absolute (contoured) escape fraction. Colors as in fig. 1

assuming a magnification of 10, this corresponds to a source-plane diameter of ∼ 160 pc. If the magnification is stronger, the scale of the emitting region will drop by a factor of a few to ∼ 50 – 100 pc. This compares reasonably well with star forming regions in local galaxies[14]. At larger redshifts, star forming clumps of down to ∼ 30 pc have been observed[14,18]. In the absence of any measurable shear, this is an upper limit to the size. It is however clear that the size of the emitting region is consistent with typical scales of star forming regions in well studied galaxies.

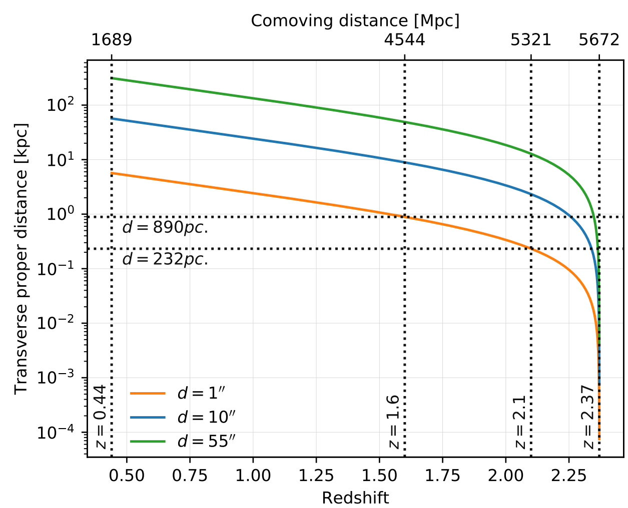

Figure 3: Transverse physical distances between lines of sight separated by 1, 10 and 55” in the lensing plane as a function of redshift.

The multiply imaged ionizing source could also enable probing neutral intergalactic gas on transverse scales an order of magnitude smaller than so far seen[15]. The fact that the differing values of $f^{*}_{\mathrm{esc,rel}}$ are measured from the same source means that the different absorption of ionizing photons must happen en route from the emitting region. As explained in the Methods section, this absorption *must* occur at redshifts above $\gtrsim 1.6$, and most likely occurs at a redshift $\gtrsim 2.1$, below which all the intrinsically ionizing photons observed in F275W have redshifted below the ionization wavelength of Hydrogen. In fig. 3, we show the transverse distance between lines of sight to images 2 and 3 (orange), 1 and 6 (blue), and 1 and 12 (green) as a function of redshift, and mark the transverse distance between the lines of sight to images 2 and 3 at redshifts 1.6 and 2.1. If the gas is absorbed outside the galaxy, it can be due to either an undetected, interloping galaxy, or a Lyman Limit system of cold intergalactic gas. Of these, the latter are the more numerous and better in line with the apparent absence of a multiply imaged foreground system, but neither can be ruled out without further analysis. If on the other hand the light is absorbed within the galaxy, the transverse scale is much smaller; at a distance from the source of ~ 10 kpc, comparable to the size of a star forming galaxy at these redshifts, the transverse distance between lines of sight of images 2 and 3 is a few percent of a parsec, a small fraction of the distance from the Sun to the nearest star. It seems unlikely to find such large variation on such small scales, but with our current knowledge of ISM structure, it cannot be ruled out.

These findings show that the Sunburst Arc is interesting as more than just the brightest known lensed arc. It demonstrates a mode of escape of ionizing photons previously theorized, but never before conclusively observed, and thus provides a benchmark for models of ionizing photon escape. It probes neutral intergalactic Hydrogen on transverse scales not accomplished before. The brightness and direct escape of the ionizing photons could enable the first ever measurements of the extreme UV spectrum of the very hottest O-type stars; a feat which so far has not even been accomplished inside the Milky Way. Further studies of the ISM and stellar properties of the galaxy will help us understand how it fits into the bigger picture of how ionizing photons escape their galaxies and ionized the intergalactic gas in the early Universe.

References

[1] Leitet, E., Bergvall, N., Hayes, M., Linné, S. & Zackrisson, E. Escape of Lyman continuum radiation from local galaxies. Detection of leakage from the young starburst Tol 1247-232. A&A **553**, A106 (2013). 1302.6971.

[2] Izotov, Y. I. *et al.* Low-redshift Lyman continuum leaking galaxies with high [O III]/[O II] ratios. MNRAS (2018). 1805.09865.

[3] Borthakur, S., Heckman, T. M., Leitherer, C. & Overzier, R. A. A local clue to the reionization of the universe. *Science* **346**, 216–219 (2014). 1410.3511.

[4] Vanzella, E. *et al.* Hubble Imaging of the Ionizing Radiation from a Star-forming Galaxy at Z=3.2 with fesc50%. ApJ **825**, 41 (2016). 1602.00688.

[5] Vanzella, E. *et al.* Direct Lyman continuum and Ly α escape observed at redshift 4. MNRAS **476**, L15–L19 (2018). 1712.07661.

[6] Shapley, A. E. *et al.* Q1549-C25: A Clean Source of Lyman-Continuum Emission at z = 3.15. ApJ **826**, L24 (2016). 1606.00443.

[7] Bian, F., Fan, X., McGreer, I., Cai, Z. & Jiang, L. High Lyman Continuum Escape Fraction in a Lensed Young Compact Dwarf Galaxy at z = 2.5. ApJ **837**, L12 (2017). 1702.06540.

[8] Jaskot, A. E. & Oey, M. S. Linking Lyα and Low-ionization Transitions at Low Optical Depth. ApJ **791**, L19 (2014). 1406.4413.

[9] Behrens, C., Dijkstra, M. & Niemeyer, J. C. Beamed Lyα emission through outflow-driven cavities. A&A **563**, A77 (2014). 1401.4860.

[10] Herenz, E. C. *et al.* VLT/MUSE illuminates possible channels for Lyman continuum escape in the halo of SBS 0335-52E. A&A **606**, L11 (2017).

[11] Rivera-Thorsen, T. E. *et al.* The Sunburst Arc: Direct Lyman α escape observed in the brightest known lensed galaxy. A&A **608**, L4 (2017). 1710.09482.

[12] Chisholm, J. *et al.* Accurately predicting the escape fraction of ionizing photons using rest-frame ultraviolet absorption lines. A&A **616**, A30 (2018).

[13] Dahle, H. *et al.* Discovery of an exceptionally bright giant arc at z = 2.369, gravitationally lensed by the Planck cluster PSZ1 G311.65-18.48. A&A **590**, L4 (2016).

[14] Adamo, A. *et al.* High-resolution Study of the Cluster Complexes in a Lensed Spiral at Redshift 1.5: Constraints on the Bulge Formation and Disk Evolution. ApJ **766**, 105 (2013). 1302.2149.

[15] Rorai, A. *et al.* Measurement of the small-scale structure of the intergalactic medium using close quasar pairs. *Science* **356**, 418–422 (2017). 1704.08366.

[16] Bertin, E. & Arnouts, S. SExtractor: Software for source extraction. A&AS **117**, 393–404 (1996).

[17] Vasei, K. *et al.* The Lyman Continuum Escape Fraction of the Cosmic Horseshoe: A Test of Indirect Estimates. ApJ **831**, 38 (2016). 1603.02309.

[18] Johnson, T. L. *et al.* Star Formation at z = 2.481 in the Lensed Galaxy SDSS J1110+6459: Star Formation Down to 30 pc Scales. ApJ **843**, L21 (2017).

[19] Gonzaga, S. & et al. *The DrizzlePac Handbook* (2012).

[20] Deustua, S. E. *et al.* UVIS 2.0 Chip-dependent Inverse Sensitivity Values. *Sp. Telesc. WFC Instrum. Sci. Rep.* 3 (2016).

[21] Bohlin, R. C. Perfecting the photometric calibration of the ACS CCD cameras. *Astron. J.* **152**, 60 (2016).

[22] Schlegel, D. J., Finkbeiner, D. P. & Davis, M. Maps of Dust Infrared Emission for Use in Estimation of Reddening and Cosmic Microwave Background Radiation Foregrounds. ApJ **500**, 525–553 (1998). astro-ph/9710327.

[23] Cardelli, J. A., Clayton, G. C. & Mathis, J. S. The relationship between infrared, optical, and ultraviolet extinction. ApJ **345**, 245–256 (1989).

[24] Leitherer, C. *et al.* Starburst99: Synthesis Models for Galaxies with Active Star Formation. ApJS **123**, 3–40 (1999). astro-ph/9902334.

[25] de Mello, D. F., Leitherer, C. & Heckman, T. M. B Stars as a Diagnostic of Star Formation at Low and High Redshift. ApJ **530**, 251–276 (2000). astro-ph/9909513.

[26] Chisholm, J. *et al.* Scaling Relations Between Warm Galactic Outflows and Their Host Galaxies. ApJ **811**, 149 (2015). 1412.2139.

[27] Markwardt, C. B. Non-linear Least-squares Fitting in IDL with MPFIT. In Bohlender, D. A., Durand, D. & Dowler, P. (eds.) *Astronomical Data Analysis Software and Systems XVIII*, vol. 411 of *Astronomical Society of the Pacific Conference Series*, 251 (2009). 0902.2850.

[28] Reddy, N. A., Steidel, C. C., Pettini, M. & Bogosavljevic, M. Spectroscopic Measurements of the Far-Ultraviolet Dust Attenuation Curve at z 3. ApJ **828**, 107 (2016). 1606.00434.

[29] Leitherer, C. *et al.* A Library of Theoretical Ultraviolet Spectra of Massive, Hot Stars for Evolutionary Synthesis. ApJS **189**, 309–335 (2010). 1006.5624.

[30] Meynet, G., Maeder, A., Schaller, G., Schaerer, D. & Charbonnel, C. Grids of massive stars with high mass loss rates. V. From 12 to 120 $M_{sun\_}$ at Z=0.001, 0.004, 0.008, 0.020 and 0.040. A&AS **103**, 97–105 (1994).

[31] Eldridge, J. J. *et al.* Binary Population and Spectral Synthesis Version 2.1: Construction, Observational Verification, and New Results. PASA **34**, e058 (2017). 1710.02154.

[32] Kewley, L. J., Dopita, M. A., Sutherland, R. S., Heisler, C. A. & Trevena, J. Theoretical Modeling of Starburst Galaxies. ApJ **556**, 121–140 (2001). astro-ph/0106324.

[33] Kauffmann, G. *et al.* The host galaxies of active galactic nuclei. MNRAS **346**, 1055–1077 (2003). astro-ph/0304239.

[34] Kewley, L. J. *et al.* Theoretical Evolution of Optical Strong Lines across Cosmic Time. ApJ **774**, 100 (2013). 1307.0508.

Acknowledgements

Author contributions

E.R-T. wrote the paper, taking suggestions from all co-authors, in particular H.D. and M.Gr., except the "Methods" subsections "Observations and data reductions" (written by M.K.F.), and "Stellar population synthesis" (written by J.C.). E.R-T. made all figures. H.D. wrote the *HST* proposal leading to the F275W observations, assisted by E.R-T. M.K.F. reduced and combined the images in both filters. E.R-T. performed photometry and computed escape fractions based on stellar population synthesis done by J.C., based on observations made by J.R. and M.B and reduced by J.R. MIKE observations were done by M.G. K.S. created the lens model assisted by G.M.

Competing interests

The authors declare no competing interests.

Additional information

Methods

Conventions

We have assumed a flat ΛCDM cosmology with $H_0 = 70$ km s^{-1} Mpc^{-1} and $\Omega_{M,0} = 0.3$. Flux densities are given as f_λ, and magnitudes are given in the AB system.

Observations and data reduction

The arc was observed in the UVIS channel of the *Hubble Space Telescope* Wide Field Camera 3 (*HST* WFC3) and Advanced Camera for Surveys (*HST* ACS) using the F275W and F814W filters. The F275W observations, which capture Lyman continuum emission at the redshift of the arc, were carried out during two visits, one on UT 2018 April 8, and one on UT 2018 April 14. The cumulative exposure time in the F275W filter was 9422 s. In the F814W filter, eight exposures were taken for a total of 5280 s. between UT 2018 February 21 and UT 2018 February 22. All observations were conducted using a 4-point dither pattern to minimize the effects of bad pixels and to better sample the point spread function, increasing the effective resolution of the final data products. The images in each filter were aligned using the Drizzlepac[19] routine `tweakreg`, and drizzled to a common grid with a pixel size of $0.03''$ with astrodrizzle using a Gaussian kernel and a "drop size" (`final_pixfrac`) of 0.8.

Photometry

We performed photometry using the source detection and photometry software Source Extractor[16] running in dual mode using the F275W observations as the detection image. The detection frames were smoothed by a narrow kernel 1.5 pixels wide to avoid spurious detections due to single noisy pixels, but fluxes were measured in the raw science frames in both filters. We extracted the fluxes in a fixed aperture 4 pixels wide at the positions of the 12 images in both of the filters.

The aperture size was selected to to optimize the balance between maximizing signal-to-noise and robustness to aperture placement (which both favor larger apertures), and minimizing contamination by the surrounding stellar population which is detected in F814W only (favors smaller apertures). While the Lyman continuum emitting cluster complex is unresolved or barely resolved in the *HST* observations, the observations in F814W show a complex morphology of clusters and underlying, diffuse stellar population. Thus, the measured F275W/F814W colors will depend on the chosen aperture size: larger apertures will include only the faint wings of the point spread function for the point source images in F275W, while they will include a growing contribution from the non-leaking stellar population in F814W. To determine the best aperture size, we extracted fluxes and computed flux ratios for apertures sized 2, 4, 7, and 11 pixels, corresponding to approximately ½, 1, 2, 3, and 4 times the FWHM of the corrected PSF. We found that for apertures sizes $s \leq 4$ pixels, there were little difference between the measured flux ratios, reflecting that the flux inside this aperture is dominated by the leaking point sources. We thus opted for the 4 pixel aperture, to get the best possible balance between larger aperture and uncontaminated flux from the central region. We applied aperture loss corrections as prescribed in the data analysis instructions from STScI[20,21], to convert the fluxes to AB magnitudes.

Milky Way dust correction

All measured fluxes from *HST* and MagE have been corrected for Milky Way dust using a reddening value of $E(B-V) = 0.09427$[22] and assuming a Cardelli et al. extinction law[23]. The effective wavelength for each of the *HST* filters was found as the average wavelength in each filter, weighted by the products of the uncorrected STARBURST99 model spectrum and the instrument throughput.

Stellar population synthesis

Young, massive stars produce the intrinsic Lyman continuum. These stars have characteristic spectral features in the rest-frame far ultraviolet such as broad N V 1240 Å and C IV 1550 Å stellar wind profiles[24], and weak photospheric absorption lines[25]. These features constrain the age and metallicity of the stellar population, and, consequently, the intrinsic ionizing continuum.

We constrained the ionizing continuum by fitting the observed, Milky Way extinction-corrected MagE spectra[11] with fully theoretical stellar continuum models, following the methodology of Chisholm et al. 2015[26]. We used the spectral region between 1240–1900Å in the rest frame while masking regions of strong ISM absorption and emission lines as well as absorption from intervening systems. We then assumed that the far ultraviolet continuum is a discrete sum of multiple single-aged populations of O- and B-type stars. Thus, we created a linear combination of theoretical stellar templates, with ages varying between 1–40 Myr. Due to line-blanketing in the atmospheres of massive stars, the stellar metallicity also sensitively determines the ionizing continuum and we included stellar templates with metallicities of 0.05, 0.2, 0.4, 1.0, and 2.0 $Z_\odot$ to account for a wide range of possible metallicities. The final suite of models consisted of 50 stellar templates (five metallicities each with 10 possible ages) and we fit for a linear coefficient multiplied to each individual theoretical stellar template using the IDL routine MPFIT[27]. The final linear-combination of stellar models was attenuated using the attenuation law from Reddy et al. 2016[28] by fitting for the attenuation parameter that best matched the observed continuum slope.

We used the fully theoretical, high-resolution STARBURST99 stellar continuum models, compiled using the WM-BASIC method[29] with the Geneva atmospheric models with high-mass loss[30]. We assumed a Kroupa IMF, with a power-law index of 1.3 (2.3) for the low (high) mass slope, and a high-mass cut-off at 100 $M_\odot$. The fitted stellar population is dominated by a very young (a light-weighted age of 2.9 Myr), moderately metal-rich (0.56 $Z_\odot$) stellar population. We tested whether the assumed STARBURST99 theoretical stellar templates impacted the modeled ionizing continuum by fitting the observations with BPASS models[31], but we derived similar ages, metallicities, and ionizing continua, largely because the two libraries have similar O-type stellar models[31].

The high-resolution STARBURST99 models used for the fitting accurately fit the narrow observed spectral features, but do not extend blueward of 900Å into the Lyman continuum[29]. Once we fit for the linear coefficients of the high-resolution models, we created a low-resolution STARBURST99 model using the same linear coefficients, with and without attenuation. The extinction-free template models the intrinsic ionizing continuum and allows us to compare the modeled and observed Lyman continuum.

Non-ionizing contamination in F275W

A small, but non-negligible amount of the light in F275W is transmitted redward of the observed wavelength of the Lyman edge. To ensure we are not just observing non-ionizing continuum, we have computed the expected flux in the filter by multiplying the synthetic STARBURST99 spectrum by the transmission curve of F275W and integrating this on the red side of the Lyman edge only. The derived fluxes, which span from $\sim 2\%$ to $\sim 10\%$ of the measured fluxes, were then subtracted from the measured F275W fluxes to correct for the contamination. All properties derived from measured F275W are corrected for this effect.

Ionizing escape fractions

The relative and absolute LyC escape fraction are defined as the fractions of intrinsic photons that escape the gas (and dust) of the source galaxy and reaches intergalactic Space. We have computed this based on the synthetic dust-absorbed and intrinsic spectra resulting from the stellar population modelling described above. Focusing on the *relative* escape fraction, it is defined as:

$$f_{\mathrm{esc,rel}} = \frac{F_{275}^{\mathrm{obs}}}{F_{275}^{\mathrm{int,ext}}} \frac{1}{T_{\mathrm{IGM}}}, \qquad (1)$$

where the numerator in the first fraction is the observed flux in the F275W filter, and the denominator is the same as we would see it through a completely ionized (but *not* dust-free) medium. We do not know $F_{275}^{\mathrm{int,ext}}$ directly, but since the non-ionizing continuum in F814W is unaffected by neutral Hydrogen, we can use the theoretical spectra to compute an expected flux in F275W assuming complete transparency to LyC:

$$F_{275}^{\mathrm{int,ext}} = \int L_{\mathrm{S99}} T_{275} d\lambda \frac{F_{814\mathrm{W}}^{\mathrm{obs}}}{\int L_{\mathrm{S99}} T_{814} d\lambda} \frac{\int T_{814} d\lambda}{\int T_{275} d\lambda}, \qquad (2)$$

where $L_{\mathrm{S99}}(\lambda)$ is the theoretical spectral flux density from STARBURST99, and $T_{***}(\lambda)$ are the system transmission curves for the two filters. Plugging this into eq. 1 and rearranging, we get:

$$f_{\mathrm{esc,rel}} T_{\mathrm{IGM}} = \frac{F_{275}}{F_{814}} \frac{\int T_{275} d\lambda}{\int T_{814} d\lambda} \frac{\int L_{\mathrm{S99}} T_{814} d\lambda}{\int L_{\mathrm{S99}} T_{275} d\lambda} \qquad (3)$$

We find the absolute escape fraction by the same procedure for the unattenuated theoretical spectra from SB99.

The escape fractions found this way are what we call the *apparent escape fractions*, as they do not account for absorption in the intergalactic medium. For each lensed image, they are shown in fig. 2 as filled (relative) and empty (absolute) circles.

Transmission in the intergalactic medium

To estimate the IGM transmission, we have adopted the IGM transmission distribution from Vasei et al. 2016[17], in which the authors measure the IGM transmission out to $z = 2.38$ along a large number of simulated lines of sight. This redshift is practically identical to that of the Sunburst Arc, so their coefficients can be adopted without modifications. Simply adopting the median coefficient $T_{\rm IGM} = 0.4$ from that study yields a relative escape fraction for the Sunburst Arc of more than 120%. In fact, all coefficients $T_{\rm IGM} \lesssim 0.48$ are excluded from our study, because they would yield escape fractions larger than 100%. With these values excluded, we renormalized the remaining distribution and computed the cumulative probability and found the median value with 16 and 84% confidence levels. The original and updated IGM transmission histograms, with cumulated fractions, are shown in Fig. 6. The modified distribution yielded a best value with 16th and 84th percentile confidence levels of $T_{\rm IGM} = 0.66^{+0.08}_{-0.12}$. The central vertical line in Fig. 6 mark the best value, and the shaded gray region the confidence interval. For the measured apparent escape fraction of image 12, this yields a relative escape fraction of $f_{\rm esc,\,rel} = 0.74^{+0.17}_{-0.08}$ and an absolute escape fraction of $f_{\rm esc,\,abs} = 0.30^{+0.07}_{-0.03}$.

Differential magnification

One possible explanation of the variation in the F275W/F814W flux ratios between the lensed images of the leaking region is *differential magnification*: If the sources of emission in F275W and F814W are not completely coincident (if e.g. the ionizing radiation is dominated by one massive Wolf-Rayet star located somewhat off from the central stellar component), the sources and the lens caustics might be arranged in such a way as to magnify one component significantly stronger than the other. However, this is mainly a concern when the caustics are actually crossing, or very close to, the bright sources, which makes it unlikely that this effect dominates the variations we observe. The distance between the components, if any, is unresolved in our observations and thus known to be much smaller than the distance from either to the critical lines. Still, to test this further, we consider the following:

Since the caustics do not cross the emitting region, differential magnification may only occur if one component is closer to the caustics than the other. If the center of flux in F814W is *closer* to the caustic than that of F275W, the stronger magnification of the non-ionizing flux will yield a lower apparent escape fraction, and vice versa.

This effect is somewhat counteracted by the presence of an extended stellar component surrounding the central, unresolved peak in F814W. In the case where the F275W source is more strongly magnified, a larger contribution from this extended component will be present in the aperture in F814W, but absent in F275W, and vice verse. This will counteract the effect described above. However, since gravitational lensing preserves surface brightness, the contribution from the extended component will change significantly more slowly than the main source. Thus, despite the presence of this effect, we still expect to see a strong correlation between the measured F814W flux (which is unaffected by neutral hydrogen absorption) and derived apparent escape fraction, if the effect is due to differential magnification.

In fig. 7, we show a plot of the F814W fluxes vs. the apparent escape fractions. We find only a weak correlation, with a measured Pearson's $r = 0.2$, leading us to conclude that this effect is likely not the main reason for the found variations.

Transverse scale of IGM probed by sight lines to multiple images

To calculate the transverse distances between sight lines, we used the approximation of a spherically symmetric lensing system with the telescope aligned with the source and the center of the lens. The ratio between transverse distances in the lens plane and in any plane between the source and the lens is then:

$$\frac{d_i}{d_L} = \frac{\left[1 - \frac{D_{Li} D_s}{D_{Ls} D_i}\right] D_i}{D_L}, \tag{4}$$

where d is the transverse physical distance, $D = D(z)$ is the cosmological *angular diameter distance* as a function of redshift, and the subscripts s, L and i denote source, lens, and intervening plane. In Fig.3, we plot the transverse, physical distances corresponding to $1''$, $10''$ and $55''$ in the lens plane, as function of redshift and co-moving distance. These angles are the approximate distances between images 2 and 3, across Arc 1 between images 1 and 6, and across the entire arc between images 1 and 12.

The difference in apparent escape fraction between images in the arc arises from changing column densities of neutral Hydrogen along the lines of sight. Photons of wavelength longer than the Lyman α line at $\lambda = 1216$ Å are unaffected by neutral Hydrogen, so absorption variations must occur before cosmic expansion has redshifted all the intrinsically ionizing photons beyond this wavelength.

However, the photons are much more sensitive to changes in the Hydrogen column density when they are still in the ionizing range bluer than 912 Å. Here, the optical depth depends on the logarithm of the column density. In contrast, the Lyman α line is a narrow and often saturated spectral line feature. Simply adding more Hydrogen to existing systems will have a modest effect on the total absorption. Instead, a doubling in absorption will require a doubling in the *number* of absorption systems along the line of sight, a far stronger requirement than a simple growth in column density. Recent works with close quasar pairs [15] have shown that the distribution of gas systems in the intergalactic medium is smooth on scales below 100 comoving kpc., which at this redshift corresponds to 30 kpc. physical distance, but assuming angular sizes of 1" and 10" in the lens plane, and an intermediate redshift of $z = 1.6$, makes eq. 4 yield physical transverse distances of ~ 1 and ~ 10 kpc., well below the smoothing scale. If on the other hand we assume the variation in absorption arises in the ionizing wavelength range, at redshifts $z \gtrsim 2.1$, the corresponding transverse distances are 0.2 and 2 kpc., and the gas configurations required to account for this could well be found inside one or a few absorbing systems, like e.g. the circumgalactic medium surrounding an undetected interloping galaxy, or a Lyman Limit system of cold intergalactic gas. This leads us to believe that the variations in $f^*_{\rm esc}$ most likely occur at redshifts $z \gtrsim 2.1$.

Additional figures

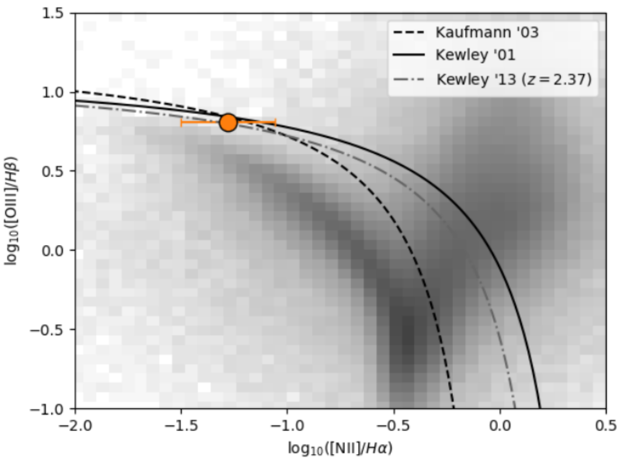

Figure 4: Baldwin, Phillips and Terlevich (BPT) diagram showing strong-line diagnostics of the Sunburst arc ionizing sources. Overlaid are the theoretical and empirical stellar/AGN separation lines of Kewley et al.[32] and Kaufmann et al.[33]. The gray-scale heat map shows 10.000 random objects from the Sloan Digital Sky Survey. The gray dash-dotted curve represents the main star formation locus at redshift 2.4 from Kewley et al. 2013[34]. Based on Magellan/FIRE spectra by Bayliss et al. (in prep).

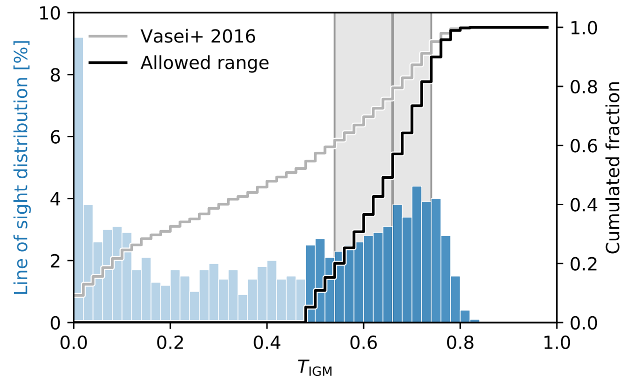

Figure 6: IGM transmission histogram by Vasei et al.[17], with unphysical values grayed out, as is their original cumulated distribution. Black steps show the updated cumulated distribution derived from the remaining, permitted values of T_{IGM}.

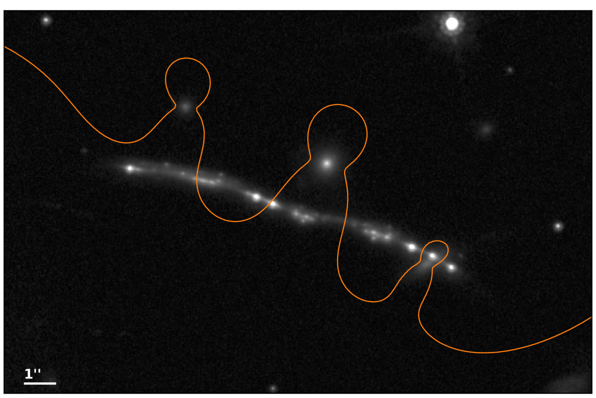

Figure 5: Critical lines in lensing model of Arc 1. This arc segment contains 6 images of the bright, leaking region.

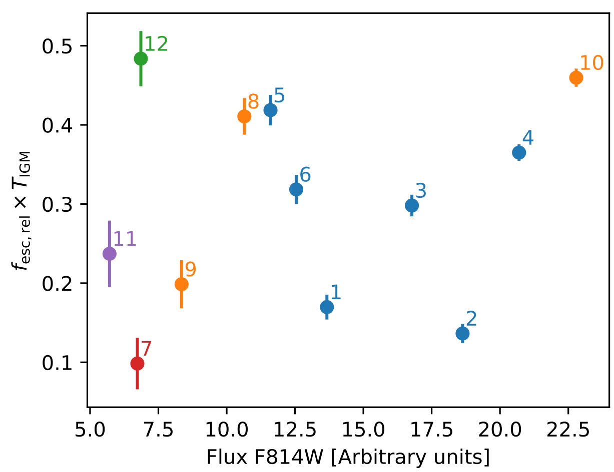

Figure 7: F_{F275W} vs. apparent escape fraction. Colors as in Figs. 1 and 2